Competing influences of greenhouse warming and aerosols

on Asian Summer Monsoon circulation and rainfall

William K.M. Lau[1,2]

Kyu-Myong Kim[3]

[1] Earth System Science Interdisciplinary Center, U. of Maryland

College Park, MD 20740

[2] Texas A&M University, Station College, Texas, 77843

[3] Climate and Radiation Laboratory, NASA/Goddard Space Flight Center

Greenbelt, MD 20771

17   *Abstract*

18   In this paper, we have compared and contrasted competing and amplifying

19   influences on the global and regional drivers, circulation and rainfall responses of the Asian

20   monsoon under global greenhouse warming (GHG) and aerosol forcing, based on CMIP5

21   historical simulations.   Under GHG-only forcing, the land warms much faster than the

22   ocean, magnifying the pre-industrial climatological land-ocean thermal contrast and

23   hemispheric asymmetry, *i.e.,* warmer northern than southern hemisphere.   A steady

24   increasing warm-ocean-warmer-land (WOWL) trend has been in effect since the 1950's

25   substantially increasing moisture transport from adjacent oceans, and enhancing rainfall

26   over the Asian monsoon regions. However, under GHG warming, increased atmospheric

27   stability due to strong reduction in mid-tropospheric and near surface relative humidity

28   coupled to an expanding subsidence areas, associated with the Deep Tropical Squeeze

29   (DTS, Lau and Kim, 2015b) strongly suppress monsoon convection and rainfall over

30   subtropical and extratropical land, leading to a weakening of the Asian monsoon

31   meridional circulation.   The inclusion of aerosol emissions strongly masks WOWL, by over

32   60% over the northern hemisphere, negating to a large extent the rainfall increase due to

33   GHG warming, and leading to a further weakening of the monsoon circulation, through

34   increasing atmospheric stability, most likely associated with aerosol solar dimming and

35   semi-direct effects. Overall, we find that GHG exerts stronger positive rainfall sensitivity,

36   but less negative circulation sensitivity in SASM compared to EASM.   In contrast, aerosols

37   exert stronger negative impacts on rainfall, but less negative impacts on circulation in

38   EASM compared to SASM.

39

1. Introduction

According to the 5th Assessment Report, Inter-governmental Panel on Climate Change (IPCC 2013), global monsoon rainfall is likely to increase, while the monsoon circulation to weaken in a warmer climate. The enhanced monsoon rainfall has been attributed to increased land-sea contrast, and more abundant precipitable water in a warmer climate, while the decreased monsoon circulation is associated with an overall weakening of the large-scale circulation required for global water balance under greenhouse gases (GHG) warming (Turner and Annamalai, 2012; Wang et al., 2012). In recent decades, while the Asian monsoon has experienced an apparent weakening in winds, it also has witnessed a general decrease in monsoon rainfall over India and persistent drought condition over northern China in conjunction with heavy rain in southern China *i.e.,* the so–called North-Dry-South-Wet (NDSW) pattern (Yu et al.,2004, 2007, Zhou et al., 2009, Lau and Kim, 2015a; Li et al., 2016).   The weakening of Asian monsoon circulation and rainfall reduction have been attributed variously to aerosol effects, sea surface temperature changes arising from GHG warming and aerosols, as well as multi-decadal natural variability (Chung and Ramanathan, 2006; Ramanathan and Carmichael, 2008; Ding et al., 2008; Zhou et al*.,* 2008; Liu et al., 2009; Cowan and Cai, 2011; Ganguly et al., 2012; Annamalai et al., 2013; Bollasina et al*.,* 2011, 2014;   Wang et al., 2013b; Lee and Wang, 2014; Cheng and Zhou, 2014, Polson et al., 2014, Lau and Kim, 2015a; Roxy et al., 2015).   On the other hand, studies have also shown that aerosols can enhance monsoon deep convection and rainfall through aerosol-cloud interactions (Rosenfeld et al., 2008; Fan et al., 2013; Li et al., 2016), and that absorbing aerosol effect can lead to increased or re-distribution of Indian monsoon rainfall depending on aerosol

63   types with different optical and physical properties, via induced dynamical feedback

64   processes, such as the Elevated Heat Pump (EHP) and related mechanisms, during different

65   phases of the monsoon season (Lau et al., 2006, 2008; Lau and Kim, 2006, 2010; Meehl et

66   al., 2008;   Randles and Ramaswamy, 2008; Wang et al., 2009; Ye et al., 2013).

67   Additionally, modeling studies have shown that the responses to the same global climate

68   change forcing from GHG and aerosols are quite different between the South Asian Summer

69   Monsoon (SASM) and the East Asian Summer Monsoon (EASM) (Menon et al., 2002; Wang

70   et al., 2013b; Zhang et al., 2009; Song et al., 2014, Li et al., 2015, Zhang and Li, 2016).

71   Because of the diverse model results and difficulty in matching long-term observations and

72   model results, unraveling the relative roles of GHG warming, aerosols, natural variability,

73   local feedback processes and differences between the SASM and EASM forcing and

74   responses remain a major challenge.   The objective of this work is to seek a more

75   fundamental understanding of climate change in the Asian monsoon regions by examining

76   the competing influences of GHG and aerosol forcing on key global and large-scale controls

77   of the entire Asian monsoon, and then elucidate differences in regional forcing and

78   feedback responses to changes in these controls.

79

80   **2. Approach and Basic Concepts**

81   Up to now, a commonly used approach for observational and modeling studies of

82   climate change in Asian monsoon regions has focused on examining changes in rainfall and

83   circulation patterns over pre-selected sub-domains within the monsoon region, usually for

84   a limited duration ($\lesssim$ 50 years). Because of the limited space-time domains chosen, the

85   difficulty in separating the myriad climate forcing (local or remote, natural and

86   anthropogenic) and the complex regional feedback processes is compounded.   More often

87   then not, these studies were carried out separate for the SASM and EASM, and did not

88   include comparing and contrasting the regional forcing and responses of the two regional

89   monsoons. In this work, we first investigate the global, zonally symmetry, and asymmetric

90   forcing by greenhouse gases and aerosols with regard to their impacts on land-sea thermal

91   contrast, relative humidity, moisture transport, and moist static energy on the Asian

92   monsoon as a whole. Then we compare and contrast the regional forcing and responses in

93   circulation and rainfall in the context of changes in these global forcing, for the SASM and

94   EASM respectively.

95   Results are based on CMIP5 historical runs for 135 years (1870-2005) under various

96   prescribed emission scenarios: 1) all forcing (ALL) including prescribed GHG, aerosol

97   emissions from historical inventories, and natural variability representing changes in solar

98   irradiance and aerosol emission from historical volcanic eruptions, 2) GHG-only, or simply

99   GHG , and 3) natural variability only. To focus on the "forced" response of the Asian

100   monsoon due to emission changes, we have minimized the impacts of model natural

101   internal variability, by constructing the Multi-Model-Mean (MMM) from an ensemble of 19

102   CMIP5 models, for all the key quantities for the June-July-August (JJA) seasonal mean. A

103   model anomaly is defined as the difference between the MMM of the last 25 years (1981-

104   2005) of the model integration, with respect to the pre-industrial (PI) control. The MMM

105   outputs for GHG-only will be used to establish the baseline of climate forcing and responses

106   of the Asian monsoon. By comparing GHG to ALL, the degree to which GHG forcing and

107   responses are masked or modulated by aerosols will be estimated. The inferred

108   anthropogenic aerosol (IAA) effect (including nonlinearity) is obtained by subtracting GHG

109   and NAT from ALL (ALL-GHG-NAT). The regional MMM rainfall and circulation responses

110   are then examined in the context of changes of key global and regional forcing, and local

111   feedback processes respectively for the SASM and EASM, based on comparison of the GHG,

112   ALL, and IAA. All models outputs have been interpolated to a global a 2.5^{o} x 2.5^{o} latitude-

113   longitude common grid. Reliability of model results is measured by a consistency test

114   defined at each grid point, by the percentage of models with anomalies having the same

115   sign as the MMM anomaly exceeding given thresholds (IPCC 2013). We use two

116   consistency thresholds, 75% (15 out of 19 models) and 65% (13 out of 19 models) in this

117   work. An assessment of the possible impacts of GHG v. aerosols forcing on Asian monsoon

118   based on comparison of MMM rainfall anomaly to observations from APHRODITE (Yatagai

119   et al., 2012) is also presented.

120

121   *2.1 Basic concepts*

122   To facilitate the discussion of results, we first present a rudimentary but important

123   concept of heating balance in the tropics. In a moisture-rich tropical environment, typical

124   of the monsoon, an approximate heat balance in the atmosphere is between diabatic

125   heating, Q and adiabatic cooling by the large-scale vertical motion w, *i.e.,* $-w\Gamma_e \approx \frac{Q}{C_p}$,

126   where Γ_e is the moist adiabatic lapse rate, C_p the heat capacity at constant pressure

127   (Holton 1992). In monsoon regions, where generally the mean vertical motion is positive

128   (w>0), and diabatic heating due mostly to latent heating, we have $Q \approx L_s P$, and $wM \approx$

129   P, where $M = -\frac{C_p}{L_s}\Gamma_e$ is the moist stability parameter. Differentiating we have:

130
$$\frac{\Delta P}{P} \approx \frac{\Delta w}{w} + \frac{\Delta M}{M} \qquad\qquad (1)$$

131

132 where the first term on the right represents changes in dynamics, and the second term

133 changes in thermodynamics. For increased (decreased) moist stability, $\Delta M < 0$ ($\Delta M > 0$).

134 Eq (1) indicates that in monsoon regions, precipitation change is a function of both

135 dynamics (circulation) and thermodynamics (moist stability). As such, increased

136 precipitation can co-exist with a weakened monsoon circulation, provided moist stability is

137 increased, or vice versa. Eq (1) will be used to quantify the relationship among circulation,

138 rainfall and stability under GHG and aerosol forcing respectively, for the SASM and EASM

139 (See Section 3.3c).

140

141 **3. Results**

142   In the next two sub-sections, we will examine the global forcing of the monsoon. For a

143 given climate system, the total forcing F can be expressed as:

144 $$F(\phi, \lambda, z) = \bar{\bar{F}} + \bar{F}(\phi, z) + \tilde{F}(\phi, \lambda, z) \qquad (2)$$

145 where ϕ=latitude, λ=longitude, z= height, consisting of $\bar{\bar{F}}$, the global mean, $\bar{F}$, the zonally

146 symmetric, and $\tilde{F}$, the zonally asymmetric components. Since the monsoon is driven by

147 thermal contrasts, only the zonally symmetric, and asymmetric components are important.

148 We will start with the zonally asymmetric component global forcing.

149

150 *3.1 Land-Sea thermal contrast*

151   It is well known that one of the main drivers of the monsoon is the large-scale land-

152 sea thermal contrast (Lau and Li, 1984; Li and Yanai, 1996; Webster et al., 1998, and many

153 others). An increase land-sea contrast will increase moisture transport from ocean to land

154 over the Asian monsoon regions (See discussion Section 3.3). During JJA, under GHG, the

155   surface temperature rises everywhere, but with more warming over the land than the

156   ocean, due to the much larger heat capacity of the ocean (Fig. 1a). The most pronounced

157   warming is found over the extratropical land regions of northern Eurasia and North

158   America and Greenland, around the Arctic Circle in northern hemisphere, and in the

159   Antarctic because of strong ice-snow albedo feedback (Dickenson et al., 1987).   Over the

160   subtropical and tropical regions, the land areas of both hemispheres are also warmer than

161   the surrounding oceans.   Overall, the GHG warming is asymmetric, with stronger warming

162   in the Northern Hemisphere (NH) than in the Southern Hemisphere (SH). Under ALL (Fig.

163   1b), the warming over both global land and oceans are more subdued compared to GHG,

164   reflecting the "masking" effect by aerosols (Ramanathan and Feng, 2009). For quantitative

165   comparison, we define the "aerosol masking effect" as:

166    $$AME = \left[1 - \frac{\Delta T_{s,ALL}}{\Delta T_{s,GHG}} \right] \qquad\qquad (3)$$

167   where ΔT_s is the surface temperature for the GHG-only and ALL experiments respectively

168   as indicated by the subscript. AME has been computed for land, and ocean, and for the

169   northern (NH) and southern hemisphere (SH) separately (Table 1).   Globally, AME is

170   large, masking 58% and 49% of the GHG warming over land and ocean respectively. AME

171   is stronger in NH (62 % for land, 62% for ocean) than the SH (45% for land, 36% for

172   ocean), reflecting strong hemispheric asymmetry due to higher level of aerosol emission

173   and loading in the NH.   The importance of the hemispheric thermal asymmetry in driving

174   the global monsoons of both hemispheres in terms of strong cross-equatorial moisture

175   transport has been noted in previous studies (Wang et al., 2013a; Lee and Wang, 2014),

176   and will be addressed in Section 3.3

177   Focusing on the differential warming between the land and ocean as a global

178   monsoon driver, we define a Warm-Ocean-Warmer-Land (WOWL) monsoon forcing as the

179   land-sea surface temperature difference 10^oS-30^oN. Under GHG, WOWL, averaged over the

180   last 25 years (1991-2005) of the model integration, increases by 0.42^o C relative to PI, with

181   the fastest rate ($\sim 0.07^o$ C per decade) during 1950-2005 (Fig.1c). Under ALL, the rate of

182   WOWL increase is much slower ($\sim 0.038^o$C per decade) for the same period, culminating in

183   an increase of approximately 0.19^o C in the last 25 years compared to PI, indicating a strong

184   AME of approximately 54%. Natural variability (NAT) shows a weak negative WOWL

185   during the last 5 decades, possibly due to the enhanced land cooling by sulfate aerosols

186   injected from strong volcanic eruptions during this period (Robock, 2000, Man et al., 2014).

187   The IAA effect, obtained by subtracting NAT and GHG from All, shows a strong negative

188   WOWL during the last 25 years with a pronounced trend ($\sim -0.0275^o$C per decade) since

189   1950, coinciding with the post-war rapid modernization of the modern era

190

191   *3.2 Global drying under GHG warming*

192   Recent observational and global climate model studies have suggested that GHG

193   warming is associated with overall drying of the subtropical and extratropical continents

194   (Dai 2006, 2011; Sherwood et al., 2010; Lau et al., 2013; Fu and Feng, 2014). Particularly

195   relevant to the ensuing analysis, Lau and Kim (2015b) has found that under GHG warming,

196   a characteristic signature in change of the global water cycle is an quasi-zonally symmetric

197   drying of the subtropical and extratropical mid- and-lower troposphere, in association with

198   a tightening of the ascending branch of the Hadley Circulation (HC), deeper convection over

199   the equatorial central and eastern Pacific, coupled to increased subsidence and widening of

200   the subtropical dry zone - the so-called Deep Tropical Squeeze (DTS) . We have computed

201   the tropospheric drying pattern for JJA in the form of a height-latitude zonally averaged

202   relative humidity (RH) anomalies under GHG and ALL forcing respectively (Fig. 2).   Under

203   GHG-only forcing (Fig. 2a), the overall drying (δRH<0) in the upper troposphere in the deep

204   tropics, in the mid- and lower troposphere in the subtropics and mid-latitude are very

205   pronounced. In the northern hemisphere monsoon subtropics and mid-latitudes of major

206   continental land regions (20-50°N), the drying extends downward to the earth surface.   On

207   the other hand, moistening (δRH>0) in the lower troposphere and near the surface is found

208   over the deep tropics and polar region, in conjunction with increased precipitation over

209   these regions (Lau et al., 2013).   Under GHG forcing, the warming of upper troposphere is

210   stronger compared to that of lower troposphere because of the moist adiabatic effect

211   (Holton, 1992). The reduction in RH can also be understood in terms of the Clausius

212   Clapyeron relationship, involving relative humidity:

213    $$\delta RH = \frac{\delta q}{q_s} - \alpha . RH . \delta T \qquad\qquad (4)$$

214   where α=L(R$_v$ T^2)$^{-1}$ ~ 6.5% K^{-1} , and q_s is the saturated vapor pressure, R$_v$ the ideal gas

215   constant, and T is the ambient temperature. From Eq (4), it can readily be deduced that a

216   faster increase in temperature compared to increase in moisture can lead to a reduction in

217   RH.   This is the reason for strong RH reduction in the lower troposphere and near the

218   surface in the northern hemisphere subtropics and mid-latitudes (25-50°N) under GHG

219   warming, because of presence of much warmer continental land mass over these latitudes.

220   The increase in RH near the tropopause and above is contributed by the warming of the

221   troposphere and cooling of the stratosphere – a fingerprint of the GHG warming (Santers

222   et al., 2012). Under All (Fig. 2b), the GHG warming fingerprint in RH is still discernable, but

223   weaker overall, reflecting strong AME due to aerosols.

224   The spatial patterns of the RH anomaly, in relations to SST and global circulation

225   anomalies under GHG and ALL are discussed next.   As shown in Fig. 3a, the 500 hPa RH

226   anomaly pattern is indeed quasi-zonally symmetric and global in extent, characterized by a

227   narrow band of increased RH over the near-equatorial regions, most pronounced over the

228   Pacific, the Atlantic and central Africa, coupled to regions of strong mid-troposphere drying

229   ($\delta RH<0$), and large-scale mid-troposphere anomalous descending motions, poleward of

230   30°N and 20°S. The most pronounced reduction in RH is found over the Southern

231   Hemisphere subtropics ($\sim 30^{o}$ S), which co-locates with the major descending branch of the

232   HC during boreal summer.   Over the northern hemisphere, the strongest RH reduction is

233   found over the subtropical and extratropical land masses of Eurasia, northeastern Asia, and

234   northern North American. RH is also reduced over the equatorial Indian Ocean, Bay of

235   Bengal, southeast Asia, and southern China, where mid-troposphere anomalous descending

236   motions prevail. This occurs in conjunction with a weakening of the Walker Circulation

237   under GHG warming (see discussion for Fig. 3d), consistent with previous studies (Vecchi

238   and Soden, 2007; Tokinaga et al., 2012).   At 850hPa (Fig. 3b), the RH-reduction regions

239   appears to further "squeeze" toward the equator, with more pronounced and widespread

240   drying ($\delta RH<0$) over the tropics and subtropics land regions of East Asia southern

241   Europe/North Africa, as well as the Americas, and adjacent oceanic regions, while the RH-

242   enhancement zones become narrower over the equatorial Pacific and central Africa/Middle

243   East region. The narrowing of the zone of increased 850hPa RH is consistent with the DTS,

244   characterized by increased subsidence on both immediate sides of the narrow zone (Fig.

245   3b), in conjunction with the development of an east-west oriented, narrow warm sea

246   surface temperature (SST) tongue (Fig. 3c) over the central and eastern equatorial Pacific.

247   The SST anomaly signals a reduced climatological east-west SST gradient along the

248   equator, which is physically consistent with a weakened Walker Circulation, featuring

249   anomalous ascent over the equatorial central and eastern Pacific, and descent over the

250   Indian Ocean and Maritime Continent region (Fig. 3d).   The widespread RH reduction and

251   anomalous subsidence in the mid-lower troposphere will suppress deep convection and

252   clouds, opposing the tendency for increased rainfall favored by increased low-level

253   moisture transported from ocean to land under GHG (See discussion in Section 3.3 and 3.4).

254   Under All, the RH anomalous patterns are similar to GHG-only with widespread

255   tropospheric drying over tropical and extratropical land and oceans at 500hPa (Fig. 3e)

256   and at 850hPa (Fig. 3f), except that wet-dry contrast is relatively weaker, with the zone of

257   positive RH near the equator broader and less well-defined compared to GHG.   Likewise,

258   the SST warm tongue and east-west SST gradient (Fig. 3g), and the anomalous rising

259   motion over the equatorial central Pacific (Fig.3h) are much less developed. These signal a

260   relatively muted development of the DTS, and reduced influence of the Walker Circulation

261   compared to GHG.   Notably, over the Asian monsoon regions, under ALL, compared to GHG

262   (Fig. 3a), the mid- and lower troposphere is even drier with expanded areas of anomalous

263   subsidence (Fig. 3e), and the anomalous subsidence over the Indian Ocean and Maritime

264   continent have intensified (Fig 3h), reflecting a strong stabilizing effect of aerosols on the

265   monsoon circulation in these regions (Bollasina et al., 2011; Lau and Kim, 2015a).

266

267   *3.3 Asian monsoon regional responses*

268   The regional responses of the Asian monsoon for the SASM and EASM are assessed

269   in light of the large-scale monsoon forcing described in previous sections.

270   *a.   Moisture transport*

271   Under GHG, the Indian Ocean and tropical Western Pacific reach a much higher

272   level of total precipitable water (TPW) due to the warmer SST, and much stronger

273   anomalous moisture transport from ocean to the Asian monsoon land stemming from

274   stronger WOWL, compared to ALL (Fig. 4). The Indian subcontinent and the Bay of Bengal

275   are moistened by increased southwesterly moisture transport which appears to originate

276   from the confluence of two distinct transport streams (Fig. 4a).   First and foremost is the

277   strengthening of the Somali Jet along the coast of East Africa, accompanied by strong cross-

278   equatorial flow, along 40-60°E, likely due to the stronger warming of the NH compared to

279   the SH (referred to Fig. 1 and Table 1).   Second is the increased westerly moisture

280   transport over central Africa (5 -15° N), from the warmer equatorial Atlantic Ocean (see Fig.

281   3c). The southwesterly moisture transport turns sharply into southerly transport over

282   southern and central China, reaching northeastern China, Korean and Japan. Here, the

283   increased southerly transport may also be contributed from increased TPW over the

284   tropical western Pacific warm pool associated with a strengthening of the Western Pacific

285   Subtropical High under GHG warming (Song et al., 2014).   Interestingly, anomalous

286   northerly moisture transport is found over the northwestern Asia including eastern

287   Eurasia toward the Asian monsoon region, implying a drying tendency over northwestern

288   Asia, and northern Eurasia.   This northerly transport coincides with regions of anomalous

289   subsidence, and reduced RH in the mid- and lower troposphere under GHG warming (See

290   Fig. 3).   Under All (Fig. 4b), the pattern of ocean-to-land moisture transport is similar to

291 GHG-only, except the magnitude is substantially reduced, due to the weakening WOWL by

292 aerosol masking effect.

293   Table 2 summarizes the changes in 850hPa moisture flux across the different key

294 cross-sections of the SASM and EASM (See Fig. 4a for geographic locations of cross-

295 sections).   Here a positive sign denotes westerly or southerly transport as appropriate for

296 each cross section.   For SASM, the PI climatology shows that the Somali jet is the primary

297 contributor of the moisture transport (+86.5 ms^{-1} gKg^{-1}) from the southern Indian Ocean

298 into the Indian subcontinent across the west coast of Indian (+110.7 ms^{-1} gKg^{-1}), while

299 moisture transport from the Atlantic Ocean across central Africa (+25.5 ms^{-1} gKg^{-1}) plays

300 a secondary role in contributing a non-negligible amount , approximately 23%, to the total

301 moisture flux into the Indian subcontinent.   For EASM, which is downstream of the SASM,

302 the moisture transport from the Indian Ocean and the tropical western Pacific across

303 central East Asia (+41.0 ms^{-1} gKg^{-1}) to northeastern East Asia (+19.8 ms^{-1} gKg^{-1}) is much

304 weaker compared to SASM. Under GHG, a large increase (8.8%) of moisture transport into

305 SASM, with substantial contribution from both the Somali jet and Central Africa.   Even

306 though the climatology moisture flux in EASM is weaker than SASM, the relative impact of

307 GHG, as measured by the percentage increase in moisture transport into East Asia, is

308 stronger, with +18.2% across central East Asia and +11.7% across northern East Asia.

309 Under ALL, all moisture fluxes remain positive, *i.e.,* enhanced relative to PI, but are

310 significantly subdued compared to GHG.   The inferred anthropogenic aerosol impact, IAA,

311 portrays a strong negative anomalous moisture transport, *i.e.*, substantially less (relative to

312 PI) moisture available for monsoon rainfall for both SASM and EASM. The IAA impact

313 appears to be stronger for EASM compared to SASM, as evident in the larger percentage

14

314   reduction of moisture transport for EASM (-21.8% for central East Asia, and -14.9% for

315   northeastern East Asia), compared to SASM   (-7.1%).

316   *a.   Moist Static Stability (MSE)*

317   To illustrate changes in the stability controls affecting the regional monsoons,

318   anomalous MSE (= C_pT +L_sq +gz), where C_p is the heat capacity at constant pressure, L_s the

319   latent heat of condensation, and z the geopotential height, has been computed for the SASM

320   (70-100°E) and EASM (100-130°E) sectors, respectively. For SASM under GHG warming,

321   the lower troposphere is conditionally unstable, as indicated by the vertical gradient of the

322   MSE.   The near surface MSE over SASM is strongly enhanced from the Indian Ocean and the

323   Indian subcontinent, up to the southern slopes of the Tibetan Plateau (Fig.5a). Separate

324   calculations (not shown) indicate that the increase in low-level MSE is due primarily to

325   moisture effect (qL_s), although temperature effect (C_pT) also contributes. However, above

326   500 hPa, the gradient of the MSE (increasing with height) indicates increased atmospheric

327   stability due mainly to moist adiabatic temperature effect from ascent of warmer air over a

328   warmer surface. Above 200 hPa, convective instability is again enhanced. Notice that the

329   mid- and upper troposphere over the Indian Ocean and southern land regions (10°S-15°N)

330   is warmer than that over the monsoon land regions to the north.   This is because of the

331   much higher TPW over the large span of the warming Indian Ocean than over monsoon

332   continental land, even though the latter is warmer than the former, *i.e.*, positive WOWL.

333   Under GHG, ascending warm moist parcels over the Indian Ocean, by conservation of MSE,

334   will convert more latent heat (moisture) to sensible heat (temperature) and thus causing

335   the upper troposphere to warm faster and more over oceans than monsoon land to the

336   north.   Past studies (Li and Yanai, 1996, and others) have shown that a stronger SASM is

337   associated with positive upper tropospheric temperature gradient, *i.e.*, warmer north,

338   cooler south.   Thus, under GHG, the tropospheric meridional temperature gradient actually

339   favors a *weaker* SASM monsoon, because the upper troposphere over the deep tropics is

340   warmer than over monsoon land, even though WOWL is positive at the surface (Fig. 1).

341   The IAA effect features a strong reduction in MSE near the surface and in the lower

342   troposphere over land (Fig. 5b). This is likely due to the reduced WOWL by strong cooling

343   of the land surface via the aerosol solar dimming effect, and the semi-direct effect in

344   increasing atmospheric stability in the lower troposphere (Allen and Sherwood, 2010).

345   For EASM (Fig. 5c and d), similar changes in MSE under GHG warming and by IAA

346   can be seen, reflecting competing stability controls within GHG, and between GHG and

347   aerosols, as in SASM.   The main difference is that in EASM, under GHG, the region of

348   increased low-level MSE extends further poleward beyond $40°N$, due to the absence of

349   topographic blocking of moisture transport by the Tibetan Plateau.   Under IAA (Fig. 5d)

350   the strongest impacts by aerosol, as reflected by the maximum reduction in low-level MSE,

351   is found near $35\text{-}50°N$, which collocates with the major industrial mega-metropolis of

352   central and northern East Asia, where aerosols emissions have been increasing steadily in

353   the last several decades (Liu et al., 2009).   Note that the regional MSE anomalies are highly

354   consistent among models under GHG-only for both SASM and EASM (Fig. 5a, c), while

355   under All, the consistency is low (Fig. 5c, d), reflecting large uncertainty in aerosol physics

356   in the models.

357

358   *c. Changes in meridional circulation, rainfall, and atmospheric stability*

359   The climatology and anomalies of the monsoon meridional circulation (MMC) and

360   rainfall will be compared and contrasted for the SASM and EASM in this subsection. For

361   SASM, the climatological MMC comprises of strong rising motions from equator to the

362   Indian subcontinent characteristic by a sharp northern boundary demarked by strong

363   rising motion over the southern slope, and the top of Tibetan Plateau near 30-35°N, and

364   weak sinking motion further north (Fig. 6a).   Strong cross-equatorial flows in the upper

365   troposphere and near the surface connect the monsoon ascending to the descending

366   branch over 20-10°S (Fig. 6a). Under GHG, increased WOWL effect drives strong low-level

367   moist transport from the ocean to the foothills of the Tibetan Plateau, increasing local MSE

368   near the surface and the lower troposphere (See discussions for Fig. 5). However, the

369   increase in local MSE does not give rise to an enhanced singular monsoonal large-scale

370   circulation, because of different stability controls in the lower to upper troposphere due to

371   local (moist adiabatic warming) and remote forcing, *i.e.*, DTS induced tropospheric RH

372   reduction and subsidence, on the Asian monsoon region.   Strong sinking motion, driven by

373   the subsiding branch of the anomalous Walker Circulation prevails over 10°S-10°N (see

374   discussion in Section 3.2).   Ascending motions north of 30°N are capped to below 400 hPa.

375   Here, the growth of deep convection is inhibited because the rising moist air associated

376   with enhanced convection from the planetary boundary layer over northern Indian and the

377   Tibetan Plateau encounters large-scale subsidence and drier mid- troposphere air aloft,

378   leading to enhanced dry entrainment and suppression of deep convection and clouds (Del

379   Genio, 2012). As a result, deep convection arising from WOWL can only break out over

380   sub-domains of the SASM, *i.e.,* 15-25°N, and 0-10°N, where convective instability

381   overcomes atmospheric stability, giving rise to the appearance of multi-cell anomalous

382 MCC south of the Tibetan Plateau, and a relatively shallow circulation cell over and north

383 of the Tibetan Plateau (Fig. 6b). In contrast, IAA sustains a pronounced weakening SASM

384 MMC, in the form of a singular reversed monsoon cell with anomalous rising motion near

385 10° S- equator, strong sink motion over the entire India subcontinent, and anomalous low

386 level moisture transport from *land to ocean* (Fig. 6c). Under GHG, rainfall is increased over

387 the entire SASM region (Fig. 6d), with maxima that match well with the regions of deep

388 ascent (Fig. 6b). Strong aerosol stabilizing effects negate all the rainfall increase due to

389 GHG, as evident in the systematically reduction of rainfall, over the entire SASM domain

390 under IAA (Fig. 6d)

391 For EASM, the climatological MMC (Fig. 6e) is similar to SASM, except with a less well-

392 defined northern boundary, characterized by gradually weakening rising motion up to

393 45^oN and beyond, due to the lack of topographic blocking by high mountains. Under GHG,

394 the MMC is dominated by strong anomalous subsidence over 10^oS- 0, due to the influence

395 of anomalous Walker Circulation. Elsewhere, anomalously weak subsidence prevails, in

396 spite of the strong transport moisture from ocean to land near the surface (Fig. 6f, see also

397 Fig. 6a). Here, deep convection and ascending motions are strongly inhibited by the

398 increase in atmospheric stability due to moist adiabatic effect, as well as the remotely

399 forced mid-tropospheric dryness over subtropical and extratropical land regions. Yet,

400 because of the pronounced increased in low-level MSE from increased moisture transport

401 associate with positive WOWL, rainfall is increased over the entire EASM domain (Fig. 7h).

402 The rainfall increase is most likely coming from shallow convection, and warm clouds. The

403 changing characteristics of monsoon rainfall under GHG and aerosol forcing is a subject of

404 an ongoing investigation to be reported in a forthcoming paper. As a result of the

405   increased stability at the mid-to-upper troposphere, GHG warming alone can have

406   competing regional effects that can lead to enhanced rainfall and a weakened MMC in

407   EASM.   Under IAA, aerosols weakens the MMC substantially, as depicted by anomalous

408   overall sinking motion over all EASM land, and anomalous low-level moisture transport

409   from land to ocean, effectively drying out the EASM (Fig. 6g), and leading to overall

410   reduction in rainfall over EASM (Fig.6h).

411   Using Eq (1), we can estimate the changes in overall stability parameter M in relation

412   to changes in monsoon rainfall (P), and circulation (W) for SASM and EASM.   As a proxy for

413   W, we use the vertical motion at 500 hPa.   Table 3 shows the anomalies in P, W and M as

414   fractional changes relative to the PI climatology, averaged over the e SASM and EASM

415   sectors respectively.   Briefly, under GHG, both monsoons show increasing rainfall coupled

416   to a weakening circulation.   However, SASM has higher GHG rainfall sensitivity (+4.13%)

417   than EASM (+2.26%), but less circulation sensitivity (-1.34%) than EASM (-3.11%).   The

418   overall change in M reflects approximately the same increase in convective stability

419   ($\Delta M/M > 0$) for both monsoon, with +5.47% for SASM and +5.37% for EASM consistent with

420   the global scale nature of the GHG forcing.   Under ALL, both SASM and EASM exhibit strong

421   aerosol effects in negating the GHG rainfall increase, and in further weakening of the

422   circulation through an increase in overall convective stability, *i.e.,* smaller values of positive

423    $\Delta M/M$ compared to GHG, for both monsoons. Specifically under ALL, aerosol effect leads to

424   rainfall reduction and circulation weakening at -5.59%, and -4.02% respectively for SASM,

425   compared to EASM at -6.01%, and -3.32% respectively.   As shown in IAA, anthropogenic

426   aerosols exert stronger stabilizing effect, *i.e.*, more negative $\Delta M/M$, for EASM (-2.69%)

427   compared to SASM (1.57%).   These similarities and contrasts in sensitivities of rainfall,

428   circulation and convective stability between SASM and EASM are likely to stem from the

429   differences in climatological mean states, regional feedback processes, which are

430   dependent on different land-sea configuration, topographic influences, and aerosol types,

431   *e.g.*, absorbing v. scattering aerosols, in these two regional monsoons (Li et al., 2016).

432
433   *d. Observed rainfall comparison*
434
435   In this subsection, we provide an assessment of the realism of the MMM rainfall

436   anomalies from GHG and ALL experiments, in comparison with observed rainfall trend

437   derived from 36 years of rainfall observations from APHRODITE

438   (Yatagai et al., 2012), which provides daily gridded rainfall at 0.25 x0.25 resolution over

439   the greater Asian monsoon land domain including Middle East, and northern Eurasia for

440   57 years (1961-2007).   Under GHG, the MMM rainfall anomaly pattern (Fig. 7a) shows

441   increased rainfall over two key regions: 1) the Indian subcontinent, the Tibetan Plateau,

442   and adjacent oceans including the Bay of Bengal, southern Arabia Sea, and the equatorial

443   Indian Ocean, and 2) the western tropical Pacific and northern Pacific over northeastern

444   China, Korea and Japan.   Rainfall increase is weak between 100-120° E, possibly due to

445   the strong influence of mid-tropospheric dryness and subsidence induced by DTS, in

446   connection with a weakening of Walker circulation under GHG warming (Fig. 3). It is also

447   noted that the consistency (> 75% of models agree in the sign of the anomaly) among

448   CMIP5 models is quite high in regions where the rainfall is substantially increased.   Under

449   ALL, the aerosol effect essentially overwhelms the GHG effect, resulting in reduced

450   precipitation over most the Asian regions, in a pattern resembling a "dry land arc"

451   following the continental outline of the Asian land mass from Northeastern China, Japan

452   and Korean, through central and eastern China, Southeast Asia, eastern India to the

453   Maritime continent, and adjacent oceans. What appears to be remnant of increased

454   rainfall due to GHG warming is only found over the tropical western Pacific.

455   Anthropogenic aerosol effects, as reflected in IAA (Fig. 7c), cause dominant reduction in

456   rainfall over the entire monsoon land and ocean regions. Noting that there are only few

457   regions in which the CMIP5 models meets the 75% consistency test (Fig. 7b), the

458   reliability of the results for ALL and for IAA is likely to be much lower than that for GHG.

459   There are similarities between ALL (Fig.7b) and observed rainfall (Fig. 7d),

460   specifically in the "dry land arc" from northeastern China, through India, Southeast Asia, to

461   the Maritime continent. However, regional details are not well matched between ALL and

462   observation. In ALL, the MMM rainfall anomaly fails to reproduce the increased rainfall

463   over central and southern China - a component of the well-known NDSW observed pattern

464   of the EASM. Over India, pockets of increased rainfall over northeastern and northwestern

465   coastal regions are not simulated. However, as indicated by the scarcity of regions

466   demonstrating model consistency, the ALL and IAA results may be subject to larger model

467   diversities and uncertainties compared to GHG. Given the large inconsistency among

468   model rainfall simulations under ALL, it is possibly that model may have been overly

469   sensitive to aerosols forcing (Anderson et al., 2003; Kiehl, 2007). Because of strong

470   dynamical feedback in the monsoon ocean-land-atmosphere system, a slightly larger

471   aerosol forcing over GHG effect could be amplified, through global-scale coupled ocean-

472   atmosphere-land feedback, into strong negative IAA rainfall anomalies over the entire

473   region.

474

475   **4. Conclusions**

476

477 We have carried out an analysis of changes and impacts of key global and regional

478 drivers for GHG warming and aerosols on the circulation and rainfall of the SASM and

479 EASM respectively, based on CMIP5 historical simulations during the boreal summer

480 season, JJA. Results show large competing influences in monsoon driver and responses

481 within GHG warming alone, and between GHG and aerosol forcing and responses, in

482 effecting changes in rainfall and circulation in Asian monsoon regions.   Key findings

483 include:

484 - GHG forcing induces a strong warm-ocean-warmer-land (WOWL) effect,

485   significantly enhancing the thermal contrast between global land and ocean,

486   and between the NH and SH in the last 5 decades, since 1950. The WOWL

487   effect is responsible for increased moisture transport from ocean to land over

488   monsoon region, but is strongly masked by aerosols, up to 60% in NH monsoon

489   land and ocean regions in recent decades.

490 - GHG forcing induces a global drying (reduction of relative humidity) tendency

491   in the mid- to-lower troposphere and near the land surface of the NH

492   subtropics and extratropics, in conjunction with the development of the Deep

493   Tropical Squeeze (DTS) - a tightening of the ascending branch of Hadley

494   Circulation coupled to a widening of the subsidence regions (Lau and Kim,

495   2015b). Anomalous subsidence is also found over the oceanic, and southern

496   land regions of the Asian monsoon associated with a weakening of the Walker

497   Circulation under global warming. The large-scale subsidence and tropospheric

498   relative humidity reduction, exert strong negative impacts *i.e.,* suppressing

499   rainfall, and weakening circulation, particularly over the Asian monsoon land

500   regions.

501   - Aerosols strongly mask the GHG WOWL effect, over 60% in the NH, thereby

502   weakening the DTS, and associated negative remote forcing of the Asian

503   monsoon. However, aerosol induced local stability via solar dimming and

504   semi-direct effects, strongly weakens the monsoon large-scale circulation,

505   negating to a large extent the tendency to increase rainfall from GHG warming.

506   - Both SASM and EASM are sensitive to anthropogenic aerosol forcing, with

507   strong reduction in rainfall and weakening of the monsoon circulation. SASM is

508   more sensitive to GHG warming in terms of enhancing rainfall, and EASM more

509   sensitive to GHG stability effect in terms of circulation weakening.

510   It is important to note that above findings are all based on CMIP5 historical

511   simulations, and relevant for anomalies of recent decades, compared to the pre-industrial

512   control. The results are only trustworthy to the extent that the MMM quantities are good

513   proxies of the real world. Comparison between ALL rainfall anomaly and APHRODITE

514   observed rainfall trend pattern does not show a good match over the Asian monsoon

515   region. The largest discrepancy is in the increased rainfall over central and southern

516   China*, i.e.*, the southern portion of the North-Dry-South-Wet long-term rainfall pattern

517   over East Asia, which are missing in the MMM. Yet, both ALL and observation, but not

518   GHG-only, show a "dry land arc" spanning northeastern Asia, western China, Indo-China

519   and the Maritime Continent, hinting at a possible aerosol induced large-scale footprint on

520   Asian monsoon rainfall.   Because there is no real world observation for GHG-only

521   forcing and response, validation is impossible. However, based on model consistency (Fig.

522   7a), the reliability of results for GHG-Only is substantially higher than the ALL

523   experiments, in agreement with previous studies (Ma et al., 2016)   This is also consistent

524   with the fact that aerosol and clouds are still the two largest sources of uncertainties in

525   CMIP5 climate models. There are other fundamental reasons why the modeled MMM

526   rainfall anomalies do not match well with observations. First among them are inadequate

527   model physics, and coarse model resolution that are incapable of simulating detailed

528   rainfall and aerosol processes, particular with respect to aerosol-cloud-monsoon

529   dynamics interactions. Another is that MMM is a measure of the forced response to

530   imposed externally prescribed emission forcing with model internal variability minimized,

531   while observations represents a singular and imperfect realization of the real world for

532   the last several decades. The observed trend is likely to be reflected as a mix of forced

533   responses and natural variability including secular long-term variations, and multi-

534   decadal oscillations that have been shown to influence long-term rainfall changes over the

535   Asian monsoon region (Wang et al., 2013; Krishnamurthy and Krishnamrthy, 2014, and

536   many others).   Our results suggest that, consistent with changes in fundamental

537   thermodynamics (temperature, moist static energy) and dynamic (circulation) controls of

538   the Asian monsoon, there are some degree of similarity between ALL and the observed

539   rainfall trends over monsoon land. This means that in recent decades, and possibly in the

540   near future, there may be emerging broad scale signals of anthropogenic forcing and

541   responses in different regions of Asian monsoon, attributable respectively to GHG,

542   aerosols or combined effects, based on physical rather than strictly statistically

543   considerations. This work represents a modest first step towards establishing a baseline

544   for a holistic understanding Asian monsoon regional climate change under GHG and

545   aerosol forcing.

546   While our results show that the global and large-scale forcing, *i.e.*, the WOWL effect,

547   hemispheric thermal asymmetry, mid-tropospheric dryness, moisture transport and

548   moist static energy, affect the Asian monsoon as a whole, the component monsoon

549   forcing and responses , i.e., SASM vs. EASM, could be quite different because of regional

550   feedback processes involving interactions of monsoon dynamics and aerosols, both

551   natural and anthropogenic, modulated by regional land-sea configuration, and orography.

552   These interactions occur on diverse spatio-temporal scales from individual clouds

553   (~hours) to climate change (>100 years) and beyond (Lau, 2014, 2016).   Therefore, it is

554   important that for future work, model experiments and observational analysis should also

555   be carried out not only for monsoon climate change, but also on intraseasonal and

556   interannual variability in order to provide better understanding of aerosol dynamical

557   feedback such as the Elevated Heat Pump (EHP) effects and related processes (Vinoj et al.,

558   2014, Jin et al., 2014, Fan et al. 2015, Kim et al., 2015, Lau et al., 2016). Even under the

559   current fast pace of industrialization, natural aerosols (desert dust, black carbon and

560   organic carbon from wildfires, and sulfates from volcanic eruptions) are still several times

561   more abundant than anthropogenic aerosols in the Asian monsoon regions (Satheesh and

562   Moorthy, 2005). They are likely to play an important role in modulating intrinsic monsoon

563   processes such as onset, breaks and extreme heavy rain events, as well as climate change.

564

565

569

570

571 **Reference**
572
573 Allen, R. J., and S. C. Sherwood, 2010: Aerosol-cloud semi-direct effect and land-sea

574 temperature contrast in a GCM. *Geophys. Res. Lett.*, **37**, L07702,

575 doi:10.1029/2010GL042759.

576 Anderson A., R. Charlson, S. Schwartz, R. Knutti, O. Boucher, H. Rodhe, and J. Heintzenberg,

577 2003: Climate Forcing by Aerosols - a Hazy Picture. *Science,* **300**, 1103-1104 DOI:

578 10.1126/science.1084777

579 Annamalai, H., J. Hafner, K. P. Sooraj, and P. Pillai, 2013: Global warming shifts the

580 monsoon circulation, drying South Asia. *J. Climate*, **26**, 2701-2718.

581 Bollasina, M. A., Y. Ming, V. Ramaswamy, M. D. Schwarzkopf, and V. Naik, 2014:

582 Contribution of local and remote anthropogenic aerosols to the twentieth century

583 weakening of the South Asian Monsoon. *Geophys. Res. Lett.,* **41**, 680–687,

584 doi:10.1002/2013GL058183.

585 Bollasina, M., Y. Ming, and V. Ramaswamy, 2011: Anthropogenic aerosols and the

586 weakening of the South Asian summer monsoon. *Science*, **334**,

587 doi:10.1126/science.1204994

588   Cheng, Q., and T. Zhou, 2014: Multidecadal Variability of North China Aridity and Its

589   Relationship to PDO during 1900–2010. *J. Climate,* **27**, 1210–1222, doi:

590   10.1175/JCLI-D-13-00235.1.

591   Chung, C. E., and V. Ramanathan, 2006: Weakening of north Indian SST gradients and the

592   monsoon rainfall in India and the Sahel. *J. Climate*, **19**, 2036-2045.

593   Cowan, T., and W. Cai, 2011: The impact of Asian and non-Asian anthropogenic aerosols on

594   20th century Asian summer monsoon. *Geophys. Res. Lett.,* **38**, L11703,

595   doi:10.1029/2011GL047268.

596   Dai, A., 2011: Drought under global warming: A review. WIREs *Climate Change,* **2**, 45–65.

597   Dai, A., 2006: Recent climatology, variability and tends in global surface humidity. *J.*

598   *Climate*, **19**, 3589-3606.

599   Del Genio, A.D., 2012: Representing the Sensitivity of Convective Cloud Systems to

600   Tropospheric Humidity in General Circulation Models. *Surv. Geophys.* **33**, 637-

601   656, doi:10.1007/s10712-011-9148-9

602   Dickinson, R.E., Meehl, G.A., and Washington, W.M., 1987: Ice-albedo feedback in a CO_2-

603   doubling simulation , *Climatic Chan*ge, **10**, 241-248, doi:10.1007/BF00143904

604   Ding, Y., Wang, Z., and Sun, Y., 2008: Inter-decadal variation of the summer precipitation in

605   East China and its association with decreasing Asian summer monsoon. Part I:

606   Observed evidences. *Int. J. Climatol.*, **28**, 1139–1161, doi:10.1002/joc.1615

607   Fan, J., L. R. Leung, D. Rosenfeld, Q. Chen, Z. Li, J. Zhang, and H. Yan , 2013: Microphysical

608   effects determine macrophysical response for aerosol impacts on deep convective

609   clouds. *Proc. Natl. Acad. Sci. U. S. A.*, **110**, E4581–90,

610   doi:10.1073/pnas.1316830110.

611   Fan, J. W., D. Rosenfeld, Y. Yang, et al., 2015: Substantial contribution of anthropogenic air

612   pollution to catastrophic floods in Southwest China. Geophys. Res. Lett., **42**, 6066–

613   6075, doi:0.1002/2015GL064479.

614   Fu, Q., and Feng, S., 2014: Responses of terrestrial aridity to global warming. *J. Geophys.*

615   *Res*., **119**, doi:10.1002/2014JD021608.

616   Ganguly, D., P. J. Rasch, H. Wang, and J.-H. Yoon, 2012: Climate response of the South Asian

617   monsoon system to anthropogenic aerosols. *J. Geophys. Res.,* **117**, D13209,

618   doi:10.1029/2012JD017508.

619   Holton, J. R., 1992: *An Introduction to Dynamic Meteorology*, 3rd Edition, Academic Press

620   Inc., ISBN 012-354355-X.

621   IPCC, 2013: *Climate Change 2013: The Physical Science Basis, the contribution of Working*

622   *Group I to the Fifth Assessment Report of the Intergovernmental Panel on Climate*

623   *Change*, edited by Stocker, T.F., D. Qin, G.-K. Plattner, M. Tignor, S.K. Allen, J.

624   Boschung, A. Nauels, Y. Xia, V. Bex and P.M. Midgley, Cambridge University Press,

625   Cambridge, UK and New York, NY, USA.

626   Jin, Q.*, J. Wei, and* Z.-L. Yang *(*2014*),* Positive response of Indian summer rainfall to Middle

627   East dust*, Geophys. Res. Lett.,* 41*,* 4068–4074*, doi:*10.1002/2014GL059980

628   Kim, M. K., W. K. M. Lau, K-M. Kim, J. Sang, Y-H Kim and W-S Lee (2015), Amplification of

629   ENSO effects on Indian summer monsoon by absorbing aerosols, *Clim. Dyn*., DOI

630   10.1007/s00382-015-2722-y

631   Kiehl, J. T., 2007: Twentieth century climate model response and climate

632   sensitivity. *Geophys. Res. Lett*., **34**, L22710, doi:10.1029/2007GL031383.

633   Krishnamurthy, L., and V. Krishnamurthy, 2014: Decadal scale oscillations and trend in

634   the Indian monsoon rainfall. *Clim Dyn,* **43**: 319-331, doi:10.1007/s00382-013-

635   1870-1

636   Lau, W. K. M., 2014: Desert Dust and Monsoon Rainfall, *Nature, Geoscience, 7, 255-256,*

637   doi:10.1038/ngeo2115

638   Lau, W. K. M., 2016: The aerosol-monsoon climate system of Asia: A new paradigm, *J.*

639   *Meteorol. Res.*, 29(6), 1–11, doi:10.1007/s13351-015-5999-1.

640   Lau, K. M., and M. T Li, 1984: The Monsoon of East-Asia - A Survey. *Bull. Amer. Meteor. Soc.*,

641   **65**, 114-125.

642   Lau, K. M., and K. M. Kim, 2006: Observational relationships between aerosol and Asian

643   monsoon   rainfall,   and   circulation,   *Geophys.   Res.   Lett.*,   **33**,   L21810,

644   doi:10.1029/2006GL027546.

645   Lau, W. K.M., and K. M. Kim, 2010: Fingerprinting the impacts of aerosols on long-term trends

646   of the Indian summer monsoon regional rainfall. *Geophys. Res. Lett*, **37,** L16705,

647   doi:10.1029/2010GL043255.

648   Lau, K. M., M. K. Kim, and K. M. Kim, 2006: Asian summer monsoon anomalies induced by

649   aerosol direct forcing: the role of the Tibetan Plateau. *Clim. Dyn.*, **26**,

650   doi:10.1007/s00382-006-0114-z.

651   Lau, W. K. M., H. T. Wu, and K-M Kim, 2013: A canonical response in rainfall characteristics

652   to global warming from CMIP5 model projections. *Geophys. Res. Lett*. 40,

653   doi:10.1002/grl.50420.

654   Lau, K.M., V. Ramanathan, G-X. Wu, Z. Li, S. C. Tsay, C. Hsu, R.Sikka, B. Holben, D. Lu, G.

655   Tartari, M. Chin, P .Koudelova, H. Chen, Y. Ma, J. Huang, K. Taniguchi, and R. Zhang ,

656   2008: The Joint Aerosol-Monsoon Experiment: A New Challenge in Monsoon

657   Climate Research. *Bull. Am. Meteor. Soc.*, **89**, 369-383, DOI:10.1175/BAMS-89-3-

658   369.

659   Lau, K. M., and K.M. Kim, 2015a: Impacts of absorbing aerosols on the Asian monsoon: An

660   Interim Assessment.   In, *World Sci. Series on Asian-Pacific Weather and Climate, Vol.*

661   *6*, *Climate Change: Decadal and Beyond,* Ed: C. P. Chang, M. Ghil, M. Latif, and J. M.

662   Wallace.

663   Lau, W. K. M., and K. M. Kim, 2015b: Robust responses of the Hadley circulation and global

664   dryness form CMIP5 model CO_2 warming projections. *Proc. Natl. Acad. Sci.,* **112**,

665   3630-3635, doi: 10.1073/pnas.1418682112.

666   Lau, W. K. M., K. M., Kim, J.J., Shi, T. Matsui, M. Chin, Q. Tan, C. Peters-Lidard, W. K. Tao,

667   2016: Impacts of aerosol–monsoon interaction on rainfall and circulation over

668   Northern India and the Himalaya Foothills. *Clim. Dym,* doi: 0.1007/s00382-016-

669   3430-y

670   Lee, J., and B. Wang, 2014: Wang, Future change of global monsoon in the CMIP5. *Clim*

671   *Dyn,* **42**: 101-119, doi:10.1007/s00382-012-1564-0.

672   Li, C., and M. Yanai, 1996: The Onset and Interannual Variability of the Asian Summer

673   Monsoon in Relation to Land–Sea Thermal Contrast. *J. Climate,* **9**, 358–375.

674   Li, X., M. Ting, C. Li, and N. Henderson (2015), Mechanisms of Asian summer monsoon

675   changes in response to anthropogenic forcing in CMIP5 models, *J. Climate*, 28, 4107–

676   4125.

677   Li, Z., W.K.-M. Lau, V. Ramanathan, G. Wu, Y. Ding, M.G. Manoj, Y. Qian, J. Li, T. Zhou, J. Fan,

678   D. Rosenfeld, Y. Ming, Y. Wang, J. Huang, B. Wang, X. Xu, S.-S., Lee, T. Takemura, K.

679   Wang, X. Xia, Y. Yin, H. Zhang, J. Guo, N. Sugimoto, J. Liu, and X. Yang, 2016: Aerosol

680   and monsoon climate interactions over Asia. *Review of Geophys.* 54, doi:10.1002/

681   2015RG000500

682   Liu, Y., J. Sun, and B. Yang, 2009: The effects of black carbon and sulphate aerosols in China

683   regions on East Asia monsoons, *Tellus, Ser. B Chem. Phys. Meteorol.*, **61**, 642-656,

684   doi:10.1111/j.1600-0889.2009.00427.x.

685   Man, W. T. Zhou, J. H. Jungclaus, 2014: Effects of large volcanic eruption on global

686   summer climate and East Asian monsoon changes during the last millenium:

687   Analysis of MPI-ESM simulations. *J. Climate*, 27, 7394-7409.

688   Meehl, G., J. Arblaster, and W. Collins, 2008: Effects of black carbon aerosols on the Indian

689   monsoon, *J. Climate*, **21**, 2869-2882, doi:10.1175/2007JCLI1777.1.

690   Menon, S., J. Hansen, L. Nazarenko, and Y. Luo, 2002: Climate effects of black carbon

691   aerosols in China and India, *Science*, **297** (5590), 2250-2253,

692   doi:10.1126/science.1075159.

693   Polson, D., M. Bollasina, G. C. Hegerl, and L. J. Wilcox, 2014: Decreased monsoon

694   precipitation in the Northern Hemisphere due to anthropogenic aerosols. *Geophys.*

695   *Res. Lett.*, **41**,6023-6029, doi:10.1002/2014GL060811.

696   Ramanathan, V., and G. Carmichael, 2008: Global and regional climate changes due to black

697   carbon, *Nat. Geosci.*, **1**, 221-227, doi:10.1038/ngeo156.

698   Ramanathan, V., and Y. Feng, 2009: Air pollution, greenhouse gases and climate change:

699   Global and regional perspectives.   *Atmos. Environ.*, **43**, 37-50,

700   doi:10.1016/j.atmosenv.2008.09.063.

701   Randles, C. A., and V. Ramaswamy, 2008: Absorbing aerosols over Asia: A Geophysical

702   Fluid Dynamics Laboratory general circulation model sensitivity study of model

703   response to aerosol optical depth and aerosol absorption, *J. Geophys. Res.*, **113**,

704   D21203, doi:10.1029/2008JD010140.

705   Robock, A., 2000: Volcanic eruptions and climate, *Rev. Geophys.*, **38**(2), 191–219,

706   doi:10.1029/1998RG000054.

707   Rosenfeld, D., U. Lohmann, G. B. Raga, C. D. O'Dowd, M. Kulmala, S. Fuzzi, A. Reissell, and M.

708   O. Andreae, 2008: Flood or drought: how do aerosols affect precipitation? *Science*,

709   **321**, 1309-1313, doi:10.1126/science.1160606.

710   Roxy, M. K., K. Ritika, P. Terray, R. Murtugudde, K. Ashok, and B. Goswami, 2015: Drying of

711   Indian subcontinent by rapid Indian Ocean warming and a weakening land-sea

712   thermal gradient. *Nature Communications*, **6**, 7423, doi:10.1038/ncomms8423.

713   Santers et al. 2013, Identifying human influences on atmospheric temperature. *Proc. Natl.*

714   *Acad. Sci.,* **110** (1) 26-33; doi:10.1073/pnas.1210514109.

715   Satheesh S. K., and K. K. Moorthy, 2005: Radiative effects of natural aerosols: A

716   review. *Atmos. Environ*. 39, 2089–2110, doi: 10.1016/j.atmosenv.

717   2004.12.029.

718   Sherwood, S. C., W. Ingram, Y. Tsushima, M. Satoh, M. Roberts, P. L. Vidale, and P. A.

719   O'Gorman, 2010: Relative humidity changes in a warmer climate. *J. Geophys. Res.*,

720   **115**, D09104, doi:10.1029/2009JD012585.

721   Song, F., T. Zhou, and Y. Qian, 2014: Responses of East Asian summer monsoon to natural

722   and anthropogenic forcings in the 17 latest CMIP5 models. *Geophys. Res. Lett.*, **41**,

723   596-603, doi:10.1002/2013GL058705.

724 Tokinaga, H, S. P. Xie, and A. Timmermann, 2012: Regional Patterns of Tropical Indo-

725   Pacific Climate Change: Evidence of the Walker Circulation Weakening. *J. Climate*,

726   **2**5, 1689- 1709, DOI: 10.1175/JCLI-D-11-00263.1.

727 Turner, A. G., and H. Annamalai, 2012: Climate change and the South Asian summer

728   monsoon. *Nature Climate Change*, **2**, 587-595, doi: 10.1038/NCLIMATE1495.

729 Vecchi, G. A., and B. J. Soden, 2007: Global Warming and the Weakening of the Tropical

730   Circulation. *J. Climate,* **20**, 4316–4340, doi: 10.1175/JCLI4258.1.

731 Vinoj, V., P. J. Rasch, H. Wang, J.-H. Yoon, P.-L. Ma, K. Landu, and B. Singh, 2014: Short-

732   term modulation of Indian summer monsoon rainfall by West Asian dust. *Nat. Geosci.*,

733   **7**, 308–314, doi:10.1038/ngeo2107

734 Wang, B. J. Liu, H. Kim, P. Webster P., and S. Yim, 2012: Recent change of the global

735   monsoon precipitation (1979–2008). *Clim Dyn,* **39**, 1123–1135.

736 Wang, C., D. Kim, A. M. L. Ekman, M. C. Barth, and P. J. Rasch, 2009: Impact of

737   anthropogenic aerosols on Indian summer monsoon. *Geophys. Res. Lett.*, **36**,

738   L21704, doi:10.1029/2009GL040114.

739 Wang, B., J. Liu, H. Kim, P. J. Webters, S-Y. Yim, and B. Xiang, 2013a: Northern Hemisphere

740   summer monsoon intensified by mega-El Niño/southern oscillation and Atlantic

741   multidecadal oscillation. *Proc. Natl. Acad. Sci.*, **110**,. 5347-5352,

742   doi:10.1073/pnas.1219405110.

743 Wang, T., H. J. Wang, O. H. Otterå, Y. Q. Gao, L. L. Suo, T. Furevik, and L. Yu, 2013b:

744   Anthropogenic agent implicated as a prime driver of shift in precipitation in

745   eastern China in the late 1970s. *Atmos. Chem. Phys.*, **13**, 12433–12450.

746   Webster, P. J., V. O. Magaña, T. N. Palmer, J. Shukla, R. A. Tomas, M. Yanai, and T.

747   Yasunari, 1998: Monsoons: Processes, predictability, and the prospects for

748   prediction, *J. Geophys. Res.*, **103**(C7), 14451–14510,

749   doi:10.1029/97JC02719.

750   Yatagai, A., K. Kamiguchi, O.Arakawa, A. Hamada, N. Yasutomi, and A. Kitoh,

751   2012: APHRODITE: Constructing a Long-Term Daily Gridded Precipitation Dataset

752   for Asia Based on a Dense Network of Rain Gauges. *Bull. Amer. Meteor.*

753   *Soc.,* **93**, 1401–1415, doi: 10.1175/BAMS-D-11-00122.1.

754   Ye, J., W. Li, L. Li, and F. Zhang, 2013: "North drying and south wetting" summer

755   precipitation trend over China and its potential linkage with aerosol loading, *Atmos.*

756   *Res.*, **125-126**, doi:10.1016/j.atmosres.2013.01.007.

757   Yu, R., B. Wang and T. Zhou, 2004: Tropospheric cooling and summer monsoon

758   weakening trend over East Asia. *Geophys. Res. Lett.*, 31,L22212,

759   doi:10.1029/2004GL021270.

760   Yu, R., and T. Zhou, 2007: Seasonality and three dimensional structure of the interdecadal

761   change in East Asian monsoon*. J. Climate*, 20, 5344-5355.

762   Zhang, H., Z. Wang, P. Guo, and Z. Wang, 2009: A modeling study of the effects of direct

763   radiative forcing due to carbonaceous aerosol on the climate in East Asia. *Adv.*

764   *Atmos. Sci.*, **26**, 57-66, doi:10.1007/s00376-009-0057-5.

765   Zhang, L., and T. Li (2016), Relative roles of anthropogenic aerosols and greenhouse gases in

766   land and oceanic monsoon changes during past 156 years in CMIP5 models, *Geophys.*

767   *Res. Lett.*, *43*, 5295–5301.

768   Zhou, T., D. Gong, J. Li and B. Li, 2009: Detecting and understanding the multi-decadal

769   variability of the East Asian Summer Monsoon: Recent progress and state of affairs.

770   *Meteorologische Zeitschrift,* 18(4), 455-467

771   Zhou, T.,R. Yu, H. Li, and B. Wang, 2008: Ocean Forcing to Changes in Global Monsoon

772   Precipitation over the Recent Half-Century. *J. Climate,* **21**, 3833–3852, doi:

773   10.1175/2008JCLI2067.1.

774

775

776 Table 1 Anomaly (°C) in MMM surface temperature (T_s) in last 25 year (1991-2005) of

777 model integration compared to climatology of pre-industrial period, computed for land

778 and ocean separately, and averaged over the globe, Northern Hemisphere and Southern

779 Hemisphere for GHG-only and ALL experiments respectively.   The aerosol masking

780 effect is defined by $AME = 1 - \frac{\Delta T_{S,ALL}}{\Delta T_{S,GHG}}$.

781

	Global		NH		SH	
	Land	Ocean	Land	Ocean	Land	Ocean
GHG	1.39±0.17	0.81±0.15	1.49±0.23	0.93±0.12	1.18±0.26	0.72±0.21
ALL	0.59±0.12	0.41±0.14	0.57±0.19	0.35±0.11	0.65±0.26	0.46±0.21
AME	0.58	0.49	0.62	0.62	0.45	0.36

782
783
784
785
786
787
788
789
790
791 Table 2   850hPa moisture flux across key cross-sections affecting the SASM (West coast

792 of India) and EASM (Central East Asia, and Northeastern Asia), for GHG-only, ALL and

793 IAA respectively. See Fig. 4 for geographic locations of cross-sections.

794

Moisture Flux (m/s g/Kg)	Mean (PI)	GHG	ALL	IAA
Central Africa	25.5	5.5 (21.5%)	2.1 (8.2%)	-3.3 (-12.7%)
Somali Jet, Equator	86.5	12.3 (14.2%)	7.7 (8.9%)	-8.6 (-9.9%)
West coast of India	110.7	9.7 (8.8%)	1.1 (1.0%)	-7.9 (-7.1%)
Central East Asia	40.9	7.4 (18.2%)	2.0 (4.9%)	-8.9 (-21.8%)
Northeastern Asia	19.8	2.3 (11.7%)	0.7 (3.3%)	-2.9 (-14.9%)

795
796

797

800 Table 3 Percentage changes of precipitation ΔP/P, meridional circulation ΔW/W (W=

801 mean vertical motion at 500 hPa), and convective instability ΔM/M (=ΔP/P - ΔW/W),

802 averaged over the monsoon domain for SASM and EASM, as well as for GHG, ALL and

803 IAA respectively.   Changes are relative to the pre-industrial climatology.

W500>0.0	SASM (70E-100E, 5N-30N)			EASM (100E-130E, 20N-45N)		
	ΔP/P	ΔW/W	ΔM/M	ΔP/P	ΔW/W	ΔM/M
GHG	4.13	-1.34	5.47	2.26	-3.11	5.37
ALL	-2.29	-5.38	3.09	-4.25	-5.94	1.69
IAA	-5.59	-4.02	-1.57	-6.01	-3.32	-2.69

798

799

804

805

806

807
808

Figure Captions

810

811 Figure 1 Spatial distribution of June-July-August MMM surface temperature anomalies

812   (^{o}C) for GHG (a), and ALL (b), and time series of warm-ocean-warmer-land

813   (WOWL) index (see text for definition) for ALL, GHG, Nat, and inferred

814   anthropogenic aerosol effects , IAA = ALL-(GHG+Nat), and pre-industrial (PI)

815   control respectively (c). Grid points where more than 75% (15 out of 19), and

816   65% (13 out of 19), of the percentage of ensemble members having the same sign

817   as the MMM anomalies are indicted by black, and open circles, respectively.

818 Figure 2 June-July-August latitude-height profiles of zonally averaged climatological

819   mean (contour) and anomalous (color) relative humidity (RH) in percentage for

820   a) GHG, and b) ALL. Grid points where more than 75% (65%) of ensemble

821   members have the same sign as the MMM anomalies are indicated by black (open)

822   circles.

823 Figure 3 Left panels showing spatial distributions of RH anomalies at a) 500 hPa, b) 850

824   hPa, c) SST anomaly (^{o}C), and d) negative anomalous vertical p-velocity (10^{-2}hPa

825   s^{-1}) for GHG, with contour showing climatology.   Right panels, e), f), g) and h) are

826   the same as corresponding left panels, except for ALL.   Green dots in a), b), e) and

827   f) denote regions of anomalous descent.

828 Figure 4   Spatial distribution of anomalous moisture transport (ms^{-1} gKg^{-1}) and 25-year

829   (1981-2005) mean distribution of total precipitable water (g Kg^{-1}) for a) GHG and

830   b) ALL.   Key cross-sections for transport of moisture to SASM and EASM are

831   shown in a).

832   Figure 5   MMM Moist Static Energy (MSE) anomalies for the SASM for a) GHG and b)

833   IAA, and same for c) and d), except for EASM.   Units in kJ/Kg.   Grid points

834   with black (open) circles indicate where more than 75% (65%) of the

835   ensemble members having the same sign as the MMM anomaly.

836   Figure 6   Left panels show spatial distribution and magnitude of June-July-August

837   vertical velocity (hPa s^{-1}) associated with the monsoon meridional

838   circulation of the SASM, for a) PI climatology, b) GHG induced anomalies, c)

839   IAA induced anomalies, and d) and rainfall anomalies due to GHG (red) and

840   due to IAA (blue), with error bars indicating model spread.   Right panels e),

841   f), g) and h) are the same as corresponding left panels, except for the EASM.

842   Figure 7   Spatial distribution of June-July-August MMM rainfall anomalies (mm) for

843   a) GHG, b) ALL, c) IAA, and d) trends (mm decade^{-1}) during 1961-2007 from

844   APHRODITE rainfall observations.   In a) and b), grid points in which more

845   than 75% of ensemble members having the same sign as the MMM anomalies

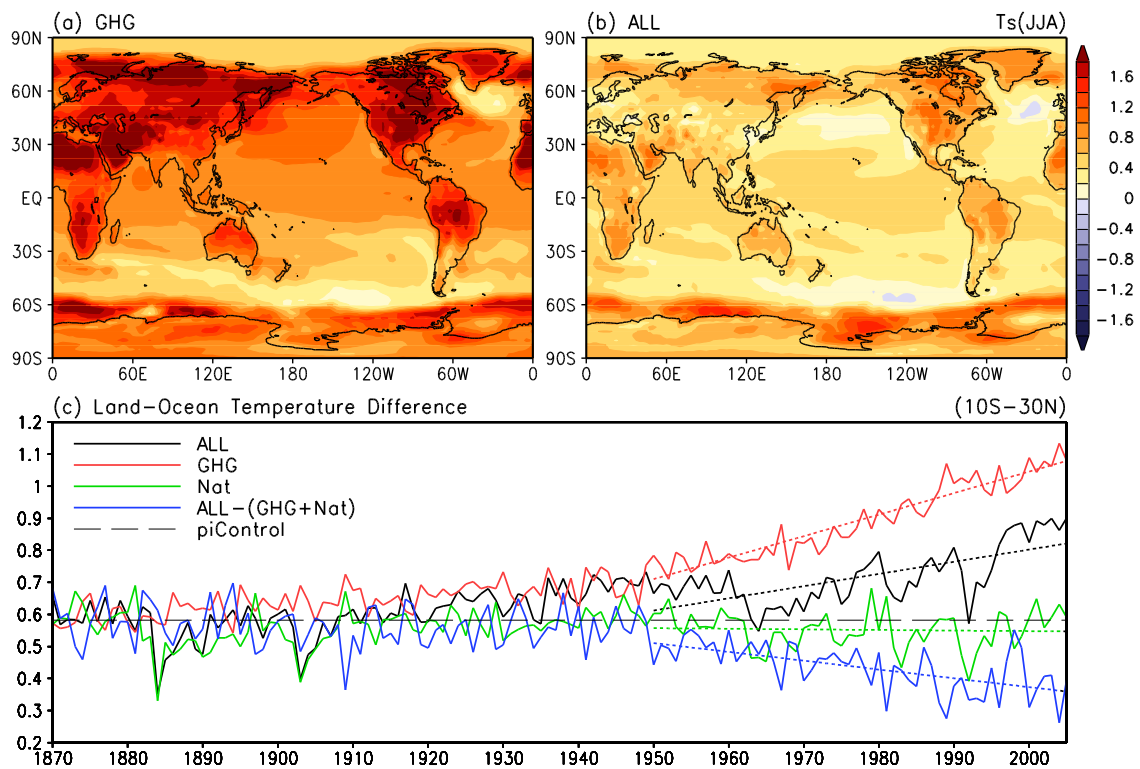846   are indicated by green solid (open) circles.
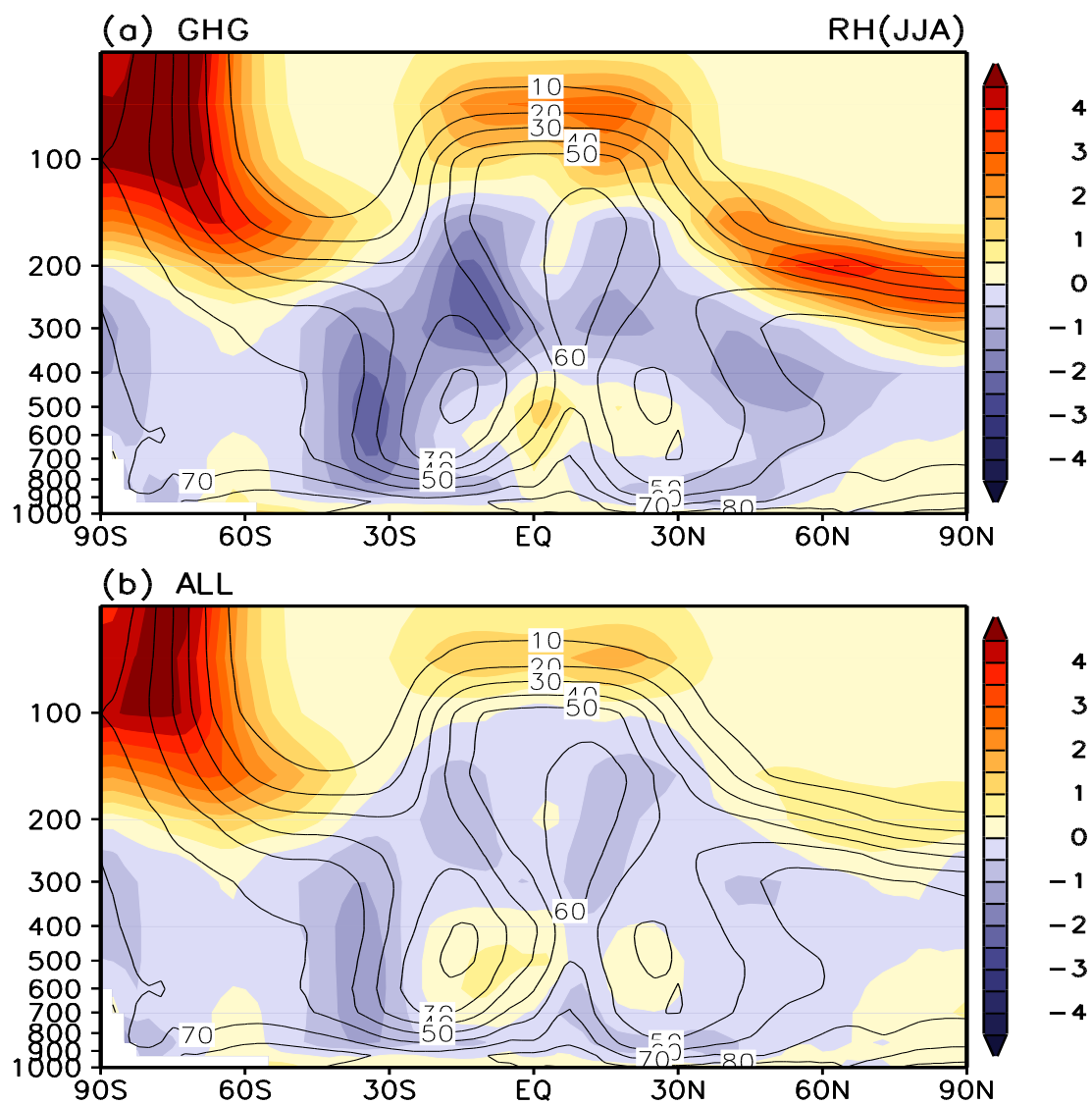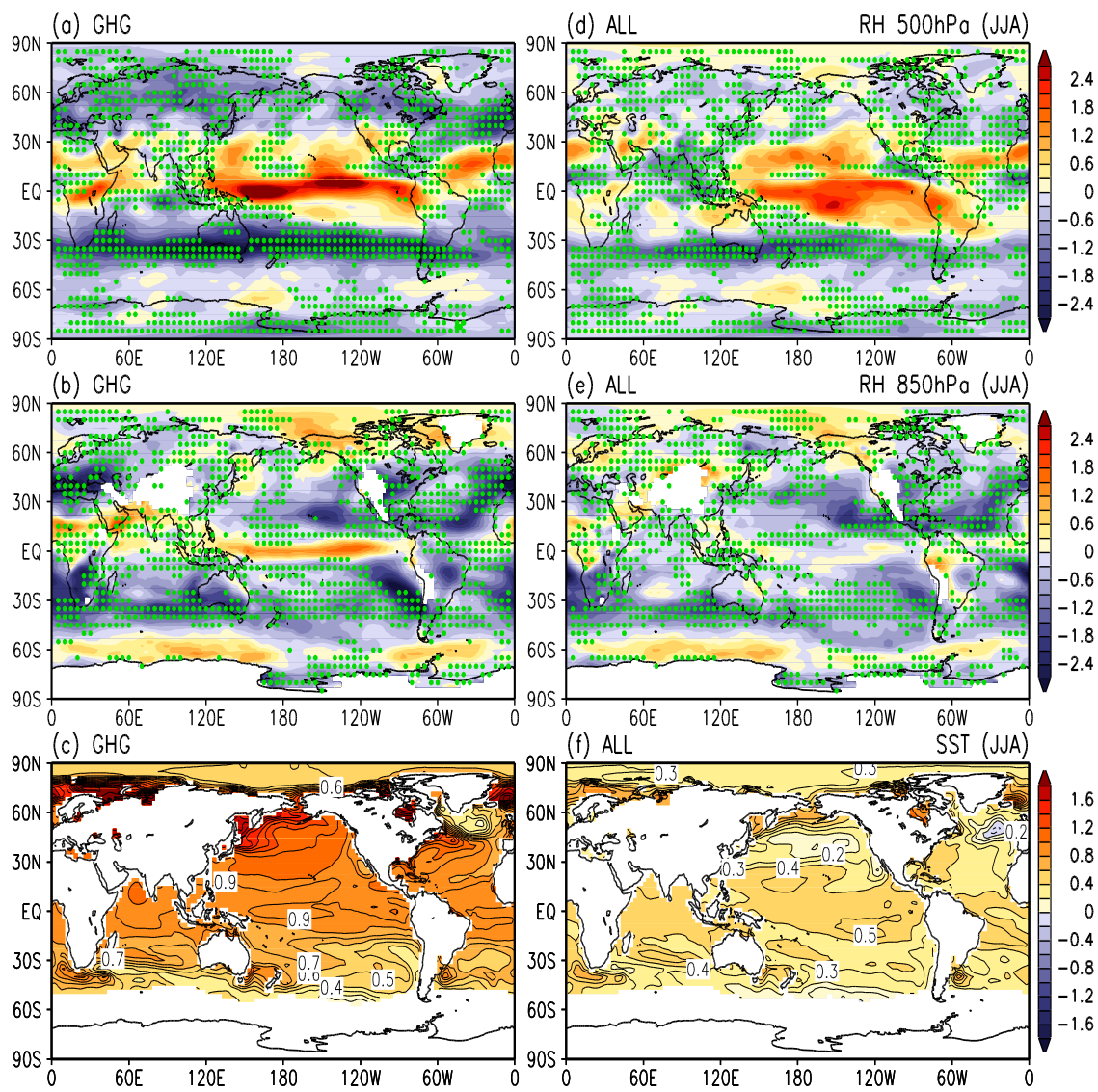
Figure 1

(a) GHG   RH(JJA)

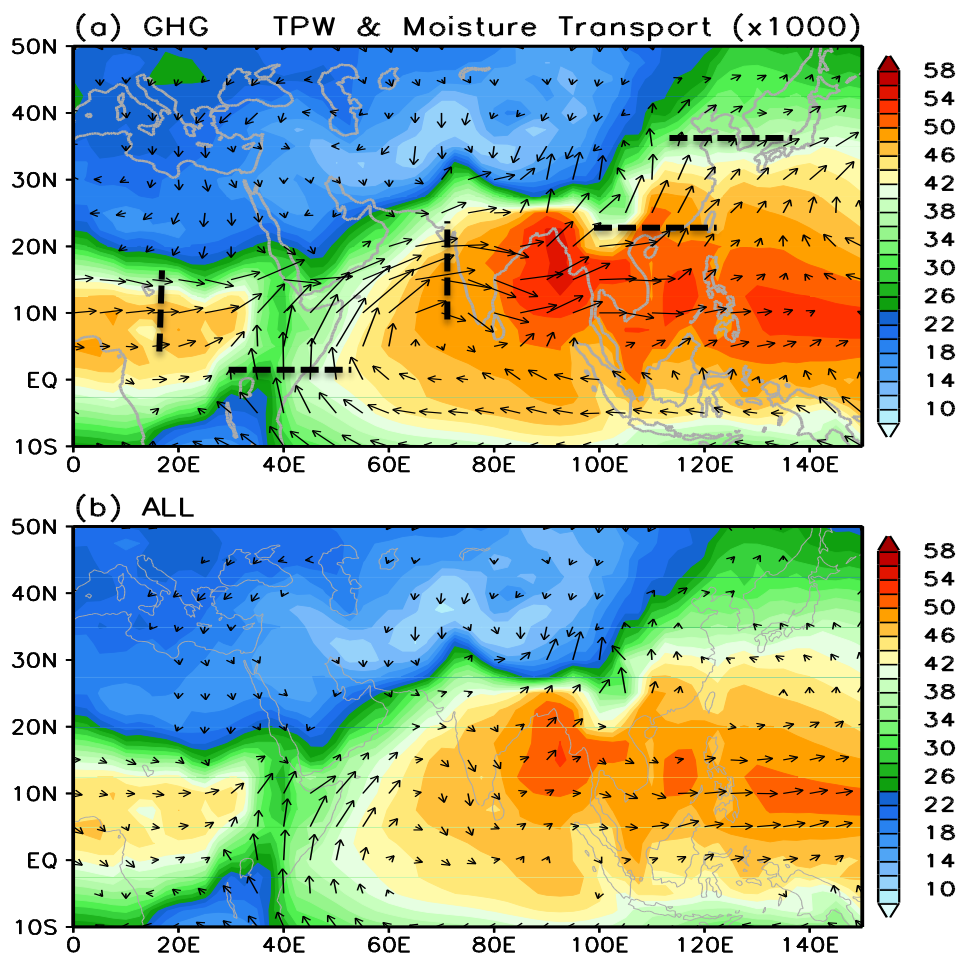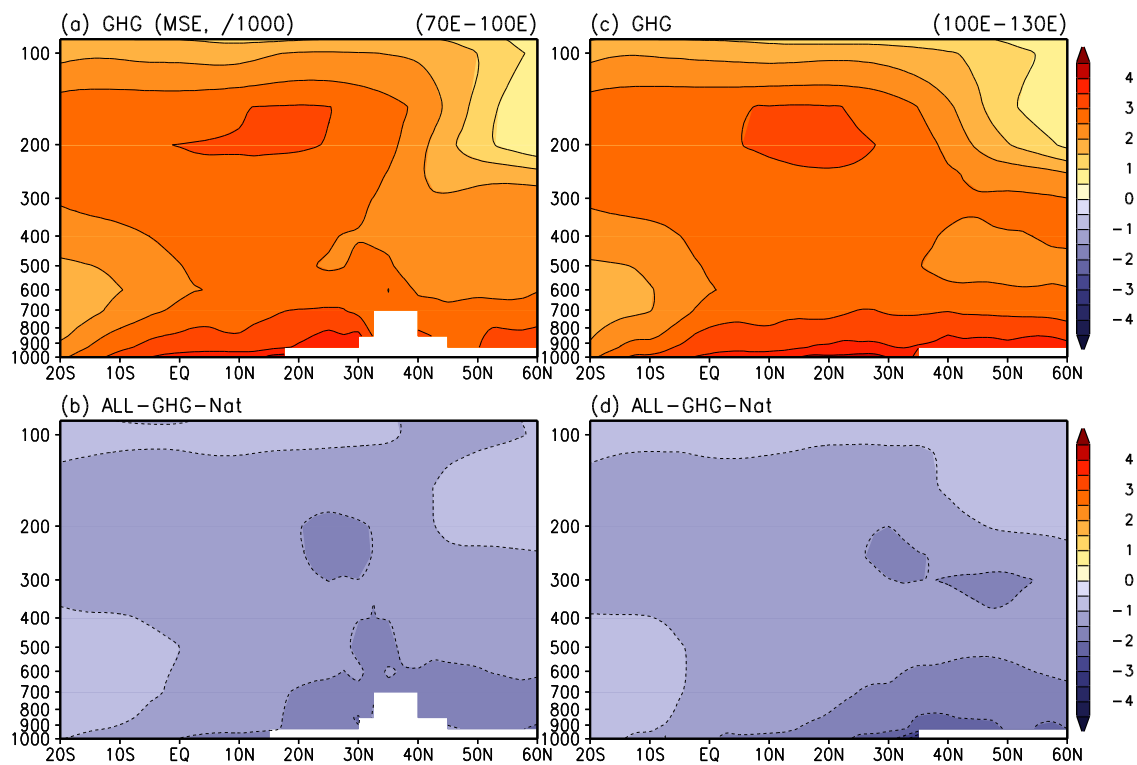(b) ALL

Figure 2

Figure 3

(a) GHG TPW & Moisture Transport (x1000)

(b) ALL

Figure 4

Figure 5

Figure 6

Figure 7